ELSEVIER

Contents lists available at ScienceDirect

International Journal of Pharmaceutics

journal homepage: www.elsevier.com/locate/ijpharm





Amphotericin B intercalated in layered clays as effective antifungal systems against eumycetoma causative agents

Alexander Misol ^{a,*,1}, Esther Sáez ^b, María Francisca Colom ^{b,c}, Margarita Darder ^{a,*}, Pilar Aranda ^a

- ^a Instituto de Ciencia de Materiales de Madrid (ICMM), CSIC, Madrid 28049, Spain
- ^b Dpto. de Producción vegetal y Microbiología, Facultad de Medicina. Universidad Miguel Hernández, Alicante 03550, Spain
- ^c NGO Research Direction, Cirugía en Turkana (Surgery in Turkana), Madrid, Spain

ARTICLE INFO

Keywords: Montmorillonite Layered double hydroxides Amphotericin B Drug delivery systems Antifungal activity Eumycetoma

ABSTRACT

Eumycetoma and other subcutaneous mycosis are severe chronic infections with a high incidence in tropical and subtropical regions, whose current treatment has a low curation rate. In the search for more effective and affordable therapies, hybrid materials based on amphotericin B (AmB), an antifungal drug with a broad spectrum of action, appear promising for localized treatment at the site of infection. In this context, the immobilization of AmB in suitable nanocarriers would be helpful to minimize its adverse side effects and ensure a controlled release over time. For this purpose, montmorillonite (MMT), showing cation exchange capacity, and layered double hydroxides (LDH), with anion exchange capacity, are explored as possible supports, taking advantage of the amphoteric character of AmB. X-ray diffraction (XRD) confirms the intercalation of AmB in both the MMT-based and LDH-based hybrids. The protective effect of the inorganic layers on the encapsulated AmB avoiding its oxidation and agglomeration is also proven. A release study from the different supports is carried out in simulated wound fluid (SWF) and in Sabouraud Dextrose Broth (SDB) growth medium, showing a sustained release for at least 60 days. Furthermore, *in vitro* tests were carried out against two causative agents of eumycetoma, *Aspergillus flavus* and *Subramaniula thielavioides* species. These results confirmed the capacity of the two layered hybrids to inhibit the growth of both fungal strains, with the LDH-based hybrid showing a stronger growth inhibition effect on *A. flavus*.

1. Introduction

Eumycetoma and Chromoblastomycosis are potentially serious, devastating, chronic, inflammatory diseases, whose worldwide incidence varies from country to country, being predominant in tropical and subtropical regions (van de Sande, 2013). These diseases affect the skin and subcutaneous tissue, damaging also the fascia, tendons, muscles and bones. Mycetoma was already described almost 200 years ago and, in 2016, the World Health Organization (WHO) included the disease, both those caused by bacteria (actinomycetoma) and fungi (eumycetoma), within the list of neglected tropical diseases (WHO, 2016). More recently, in 2022, fungi causing eumycetoma were included in a special list of dangerous fungi created by WHO (2022). Eumycetoma is caused by more than 40 species of fungi, being Madurella mycetomatis, Trematosphera grisea, and Scedosporium apiospermum the most common

causative agents of this disease (Ahmed et al., 2015; Chandler et al., 2023; Estrada et al., 2012; Welsh et al., 2014). The fungal agent is usually introduced into the subcutaneous tissue by a small trauma mainly in the foot, legs or hands, although it can also affect other parts of the body. Inside the tissue, the causative agent will organize itself into small masses called granules or grains. Thus, a small nodule will arise and gradually grow into a large subcutaneous mass with sinuses that will secrete pus and pimples. Eventually it will invade the bone and a large lesion will form, forcing amputation of the affected limb (Ahmed et al., 2004a,b; Zein et al., 2012).

Among the effective antifungals against the different varieties of fungi that cause eumycetoma, azoles such as itraconazole and ketoconazole (Ahmed et al., 2004a,b; Chandler et al., 2023), and polyenes such as amphotericin B (AmB) show the highest activity (Kloezen et al., 2018). However, the current treatments of eumycetoma are

^{*} Corresponding authors.

E-mail addresses: alexander.misol@icmm.csic.es (A. Misol), darder@icmm.csic.es (M. Darder).

Present address: Dpto. de Ingeniería Química, Universidad de Salamanca, Plaza los Caídos s/n, Salamanca, 37008, Spain.

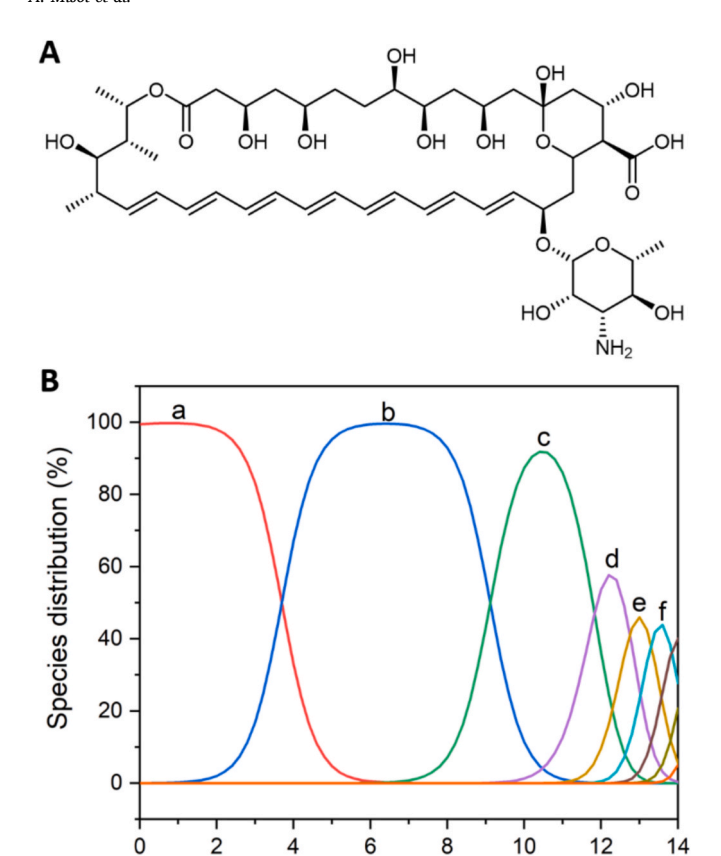


Fig. 1. (A) Chemical structure of amphotericin B and (B) distribution of amphotericin B species as a function of pH, simulated by Marvin Sketch v.6.1 software, with global charge a) +1, b) 0, c) -1, d) -2, e) -3, and f) -4. Additional details on each species are shown in Fig. S1 in Supporting information.

pН

unsatisfactory due to the low availability of antifungal drugs that can be administered to the patients without risk of side effects, and in some cases due to their high cost, and therefore, treatment with antifungals in combination with surgery is generally used to reduce the lesion size and favor the action of the drugs (Scolding et al., 2018; Sow et al., 2020; Zein et al., 2012). Unfortunately, the cure rate of current treatments do not exceed 26 % and in many cases the amputation of the affected limb is required (CDC Mycetoma, 2024; Zein et al., 2012).

AmB is a polyene antibiotic naturally produced by the actinobacteria Streptomyces nodosus, firstly isolated in 1953 and approved by the US Food and Drug Administration (FDA) as the first antifungal agent in 1965 (Gallis et al., 1990; Wang et al., 2021). It consists of a macrolactone ring conjugated to a d-mycosimine group (Fig. 1A). Due to their amphiphilic structure, it is able to bind to the lipid bilayer and form a complex with ergosterol producing pores that favor cell membrane rupture and leakage of cytoplasmic contents, leading to oxidative damage resulting in fungal cell death (Shukla et al., 2016; Wang et al., 2021). AmB is an amphoteric molecule with amphiphilic character due to the apolar and polar sides of the lactone ring and the ionizable carboxyl and amine groups. The neutral form of AmB is very poorly soluble in water; however, depending on the pH it forms different ionic species (Fig. 1B and Fig. S1 in Supporting information), thus its solubility is favored in acidic or alkaline media. Due to its low solubility and permeability, it is classified in the Biopharmaceutics Classification System (BCS) as class IV. Even though AmB is effective against a wide range of fungi and rarely encounters resistance, its use in treating eumycetoma is limited. The main reasons are that it requires prolonged intravenous administration and its dosage must be restricted due to

significant side effects, including chills, fever, nausea, hemolytic toxicity, and nephrotoxicity (Estrada et al., 2012; Gallis et al., 1990; Welsh et al., 2014). Several authors have pointed to the formation of macromolecular aggregates of AmB as dimers or tetramers as responsible for these severe harmful effects for patients (Gagos et al., 2008; Wasko et al., 2012; Yu et al., 2022), while other studies suggest that they could be rather attributed to the presence of oxidized forms of AmB, which showed a loss of antifungal properties and reduced safety in vitro (Gagoś and Czernel, 2014; Klimek et al., 2016). To overcome these drawbacks it is necessary to seek other forms of administration of this drug that could provide a safer delivery, and extend its use to the treatment of eumycetoma. For instance, as an alternative to intravenous injection, the topical administration of AmB has proven able to reduce these adverse effects in the treatment of respiratory fungal infections (Cui and Zhao, 2024; Kuiper and Ruijgrok, 2009). In addition, other delivery strategies based on the use of nanocarriers appear promising for AmB delivery with fewer side effects and greater efficacy (Dash et al., 2024; Wang et al., 2021).

The application of nanotechnology to the development of controlled drug delivery systems has been a significant development in the treatment of diseases, especially those in which the drugs produce adverse effects in the patient. These nanosized carrier systems offer multiple advantages, such as protection against drug degradation and metabolism through encapsulation, longer residence time and can be tuned to improve drug specificity to target cells or organs (Park et al., 2022; Patra et al., 2018). Natural clay minerals and synthetic layered double hydroxides (LDH) have been known for years as safe, biocompatible and low cost carriers for drug delivery and other health related applications (Aguzzi et al., 2007; Ruiz-Hitzky et al., 2019; Yang et al., 2016). LDHs are advantageous for the development of controlled drug delivery systems (Aguzzi et al., 2007), including antimicrobial drugs for the treatment of bacterial or fungal infections, due to their easy preparation, the possibility to control their composition, and their large anion exchange capacity (AEC). Among natural clay minerals, smectites such as montmorillonite (MMT) have been the most studied due to their higher cation exchange capacity (CEC) compared to other pharmaceutical silicates (Aguzzi et al., 2007).

The preparation of nanometric AmB carriers has been reported in the literature, where most of them significantly reduced side effects and increased their therapeutic effect. Among the reported nanometric systems, polymeric nanoparticles, conjugates, lipid-based delivery systems, nanoemulsions, nanosuspensions, metal-based nanoparticles and microneedles are included as the most promising AmB delivery systems (Nahar et al., 2008; Wang et al., 2021). Although clay minerals and LDH have been largely studied as nanocarriers of many drugs as mentioned above, their use for the encapsulation of AmB is still scarce and could present additional advantages to those of the most explored carriers. So far, the best reported attempt was the intercalation of AmB in a ZnAl-LDH through coadsorption with surfactants, due to the low solubility of AmB in aqueous media, although the nanohybrid materials reached a low content of encapsulated drug, below 10 % w/w (Trikeriotis and Ghanotakis, 2007).

Aiming at reducing the disadvantages of AmB for the treatment of eumycetoma, this work proposes the development of hybrid delivery systems based on the intercalation of AmB in layered materials, both a clay mineral of the smectite type, a Wyoming MMT, and a ZnAl LDH, that may protect the drug molecules keeping them in non-aggregated state and avoiding their oxidation, and allowing the controlled and extended release of this antifungal drug. Their performance will be evaluated in vitro against fungal strains of Aspergillus flavus and Subramaniula thielavioides, isolated from human eumycetoma cases from Turkana County in Northwestern Kenya (Colom et al., 2023), in order to assess the suitability of the developed materials for the effective treatment of this neglected disease.

2. Materials and methods

2.1. Starting materials

Amphotericin B from *Streptomyces* sp. $(C_{47}H_{73}NO_{17}, MW: 924.08)$ was purchased from Apollo Scientific. For the synthesis of LDHs, Zn $(NO_3)_2\cdot 6H_2O$ (98–102 %), Al $(NO_3)_3\cdot 9H_2O$ (98–102 %) and NaOH (98–100 %) were purchased from Panreac. Homoionic Na-MMT $(Na)_{0.33}(AlMg)_2(Si_4O_{10})(OH)_2\cdot nH_2O$ corresponds to a Wyoming-type smectite clay supplied by Southern Clay Products as Cloisite®Na, with a CEC of 93 meq per 100 g. Ultrapure water (conductivity >18.2 M Ω cm) was obtained from PURELAB® Chorus ELGA VEOLIA equipment. For the preparation of AmB solutions, HCl (37 %) were purchased from Panreac and dimethyl sulfoxide (DMSO) pure were purchased from Scharlau. For the preparation of release media: NaCl (99–100.5 %) and CaCl $_2\cdot 2H_2O$ (99–103 %) were purchased from Panreac; D(+)-Glucose anhydrous (dextrose 98–102 %, $C_6H_{12}O_6$, MW: 180.16) and potato peptone were purchased from Sigma-Aldrich. All reagents were used as received.

Fungal isolates: Two species of filamentous fungi were used to test the efficacy of the compounds. They were *Aspergillus flavus* and *Subramaniula thielavioides* and both were isolated from mycetoma lesions in patients treated in Turkana (North-West Kenya) by the health cooperation group Cirugía en Turkana under the direction of M.F. Colom. These isolates were phenotypically identified by macro- and microscopic characteristics, and additionally, identification was confirmed by amplification of the ITS region of the rDNA followed by blast comparison in the NCBI database (accession numbers: MG575502.1 and MG250407.1, respectively). Fungi were grown on two culture media: the natural medium Brain Heart infusion (BHI) and Sabouraud Dextrose Agar (SDA) prepared from Sabouraud Dextrose Broth (SDB) which is a semi-synthetic medium consisting of an aqueous solution of 10 g/L peptone and 20 g/L dextrose; BHI and SDB were supplied commercially by Condalab® (Madrid, Spain) and agar was supplied by Sigma-Aldrich.

2.2. Adsorption isotherm of AmB in MMT

To determine the adsorption isotherm of AmB in MMT, several AmB solutions of increasing concentration were mixed with dispersions of MMT containing the same amount of MMT. A certain amount ($\approx\!30$ mg) of the Na-MMT clay mineral was dispersed in 20 mL of water acidulated at pH 4 with 0.2 M HCl. Subsequently, variable amounts of a 20 mg/mL AmB solution in DMSO were added to the MMT dispersion, in order to have AmB concentrations ranging from 0.7 to 20 mg/mL. The mixtures were submitted to continuous stirring during 48 h at 25 °C. For each point of the adsorption isotherm, the measurements were carried out in duplicate. The MMT-AmB intercalation compounds were recovered by centrifugation at 12,000 rpm, during 10 min at 25 °C to separate the solid from the supernatant, without further washing. Then, the hybrid materials were frozen at -20 °C for 24 h and lyophilized in a FreeZone 4.5 Liter Benchtop freeze-dryer from Labconco for 2 days.

2.3. Synthesis of MMT-AmB hybrids

The intercalation of amphotericin B in Na-MMT was performed by dispersing 0.5 g of MMT in 50 mL of water acidulated at pH 4 with HCl. Subsequently, a given volume of a 20 mg/mL AmB solution in DMSO corresponding to 200 mmol of AmB per 100 g of MMT was added to the MMT dispersion. The mixture was submitted to continuous stirring during 72 h at room temperature. The MMT-AmB hybrid was recovered by centrifugation and washed four times with water. The final solid was dried by lyophilization as indicated in the previous section. Afterwards, the hybrid material was characterized by several physicochemical techniques.

2.4. Synthesis of LDH ZnAl-AmB hybrids

The samples were synthetized by the co-precipitation method at constant pH 10 (Rives, 2001). An aqueous solution of the nitrate salts of the metal cations was prepared (0.1 M, M^{II}/M^{III} molar ratio = 2/1). An aqueous AmB solution (2.8 × 10^{-3} M) was prepared by diluting in 100 mL of pure water 15 mL of a 20 mg/mL AmB solution in DMSO. The aqueous AmB solution was adjusted at pH 10 by adding 1 M NaOH solution. The synthesis started with the dropwise addition of the cation solution by means of an automatic dispensing equipment (DOSINO 800, Metrohm) that regulates the dripping at a rate of 2 mL/min. Simultaneously, the pH of the precipitation medium was kept close to 10 by adding the necessary volume of 1 M NaOH solution. The synthesis was controlled automatically by the 867 pH Module by means of the pH sensor Unitrode 854 iConnect, and using the software Tiamo ν 2.3, all of them from Metrohm. The synthesis was kept under a constant N₂ flow and was carried out at room temperature and dark conditions.

The slurry obtained was stirred under intense agitation during 12 h. Finally, the solid was separated from the aqueous phase by centrifugation at 4000 rpm, during 10 min at 25 $^{\circ}\text{C}$. The solid was washed three times with pure water until pH close to 7, in order to remove the counterions of the starting salts. The solid was dried by lyophilization process and manually ground using an agate mortar.

2.5. Characterization

Powder X-ray diffraction (XRD) data were collected in a Bruker D8-ADVANCE diffractometer equipped with a "Lynxeye" detector, using a Cu-K α radiation ($\lambda = 1.54050 \,\text{Å}$), with a scan speed of 0.1° (20) s⁻¹ between 3 and 70° (20) applying 30 mA and 40 V and a slit of 0.6 mm. To record the diffractogram at starting 2θ angle of 2° , the parameters of the equipment were modified to 15 mA and 20 V and a slit of 0.2 mm. The diffractometer was operated using the Diffrac plus XRD Commmander V2.6.1 software and the diffractograms were analyzed with the Diffrac. Eva V6.1 software, equiped with the PDF-5 + 2025 (v4.25.0.2) database; both software packages are provided by Bruker. Fourier transform infrared (FTIR) spectra were recorded with a FTIR spectrophotometer Bruker Vertex 70 V controlled by OPUS 8.2.28 software. Each sample was placed in a sample holder as KBr pellets and scanned from 4000 to 400 cm⁻¹ with 2 cm⁻¹ resolution. The amount of organic matter in the samples was determined by CHNS elemental chemical microanalyses using a LECO CHNS-932 elemental analyzer. The sodium and chloride contents were semiquantitatively determined by energy dispersive X-ray spectroscopy (EDX) using a EDAX Genesis XM2i detector, coupled to a field emission scanning electronic microscope (FESEM) FEI-Nova NanoSEM 230, operated with Genesis Spectrum 5.21 and Nova Nano-SEM 1.3 software. The thermal behavior of the different prepared mawas analyzed from the simultaneously recorded thermogravimetric (TG) and differential thermal analysis (DTA) curves using a SDT Q600-TA Instruments equipment and the Advantage software, in experiments carried out under an air atmosphere (flux of 100 mL min⁻¹) from room temperature to 800 °C at 10 °C min⁻¹ heating rate. A Shimadzu UV2401PC UV-vis spectrophotometer was utilized to register the ultraviolet-visible absorbance spectra at ambient temperature in the wavelength range between 250 and 550 nm, using the software UVProbe 2.40 from Shimadzu. Quartz cuvettes with 1 cm path length were used for the measurements. All graphical representations and nonlinear fittings of the experimental data to the proposed mathematical models were carried out using OriginPro 2024 (OriginLab Corporation, USA), which also provided the corresponding statistical parameters associated with each fit.

2.6. In vitro release of AmB and zinc ions in simulated wound fluid (SWF) and Sabouraud Dextrose Broth (SDB)

The release of bioactive components from the MMT-AmB and LDH

ZnAl-AmB hybrid materials was carried out in vitro in simulated wound fluid (SWF; 142 mM NaCl and 2.5 mM CaCl₂, pH \approx 6) (Canada et al., 2011) and Sabouraud Dextrose Broth (SDB; 40 g/L dextrose and 10 g/L peptone, pH \approx 5). The release study from the hybrid material was performed by adding a weighed amount of the hybrid material (ca. 80 mg) to 40 mL of release medium, kept under stirring at 80 rpm in a thermostatic bath (SW23, Julabo) at 35 °C. After different periods, an aliquot of 2 mL was filtered (0.45 µm) and 5-fold diluted and analyzed to determine the released amounts of AmB and zinc ions. The subtracted aliquot was restocked with the same amount of fresh medium to keep a constant volume during the release study. In the case of the release study in SWF, AmB content was measured in an Analytik Jena multi-N/C2100 total organic carbon (TOC) analyzer. The amount of AmB in the SDB release study was analyzed by UV-vis, recording the absorbance at 306 nm, and determined from the linear correlation between the absorbance values and the concentration measured by TOC of the oxidized AmB released in SWF (Fig. S2). The amount of released zinc was determined by total X-ray fluorescence in a TXRF S2 PICOFOX from Bruker. In all these studies, the experiments were carried out in duplicate. The AmB release profiles were fitted to different mathematical models detailed in the Supporting information, and the best fitting model was determined according to their statistical parameters.

2.7. In vitro determination of antifungal activity against eumycetoma causative strains

Two isolates of fungi obtained from eumycetoma lesions of patients attended in Turkana (Kenya), were used to test the effectivity of the clayantifungal compounds. The growth of Aspergillus flavus and Subramaniula thielavoides were carried out by inoculation on two mycological media: SDA and semi-solid BHI. The inhibition tests were studied by fungi growth in the presence of MMT-AmB and LDH ZnAl-AmB. The inoculum consisted of conidia suspended in sterile saline solution at a concentration of about 10⁴ cells/ml adjusted by turbidity (MacFarland scale 0.5). In the solid medium the fungus was inoculated onto the SDA plate and spread with a Drigalski seeding loop. The hybrid compounds were added to the inoculated media by depositing a 5 µL liquid droplet with the corresponding amount of hybrid material at a concentration of $0.1~mg/\mu L$ AmB on the surface. The established therapeutic doses for amphotericin B administered by intravenous infusion (1.5 mg/kg/day) and those considered for local injection (e.g. intravitreal: $5-10~\mu g$) have been considered as indicators of the dose to be tested in the in vitro assays (Noor and Preuss, 2024). With these data and considering the release capacity of the compound from MMT and LDH, we calculated the deposition of a 5 µL drop of compound corresponding to approximately 200 µg of AmB. Taking into account the release capacity of the compounds from the clays and LDH, we estimated an average drug release in situ of about 30-35 µg. Given the fungal inocula and AmB doses on which standardised antifungal susceptibility testing is based, following the European Committee on Antimicrobial Susceptibility Testing (EUCAST) protocols (EUCAST, 2011), we consider that the AmB dose tested was appropriately adjusted.

On the other hand, for the semi-solid BHI medium, the inoculum was mixed with the medium at a temperature of about 60 $^{\circ}$ C and allowed to cool and solidify in petri dishes and then deposit liquid droplets of the product on the surface. Inhibition of growth around the products was compared to negative controls. The experiments were performed three times for each fungus and each hybrid compound.

3. Results and discussion

3.1. Synthesis and characterization of the MMT-AmB hybrid system

With the aim of evaluating the affinity of AmB for the MMT clay mineral, an adsorption isotherm was obtained to determine the maximum amount of AmB adsorbed by the silicate. Profiting from the

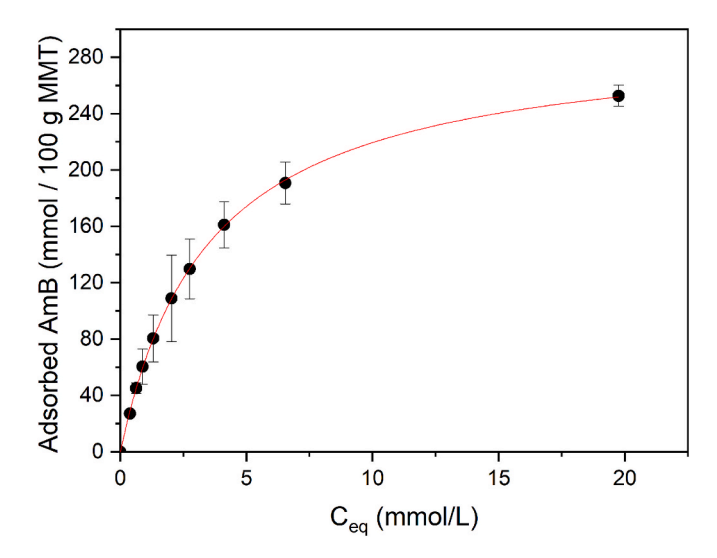


Fig. 2. Adsorption isotherm at 25 °C of AmB in Na-MMT.

amphoteric character of AmB, this molecule in cationic form was spontaneously adsorbed in MMT from $\rm H_2O/DMSO$ solutions of AmB, resulting in the adsorption isotherm obtained at 25 $^{\circ}C$ shown in Fig. 2. The adsorbed amounts of AmB for each concentration were calculated from the CHNS elemental analysis of the different solid samples. The results obtained can be fitted to a L-type (Langmuir) adsorption (Eq. (1)) according to the Giles' classification,

$$r = \frac{bx_m C_s}{l + bC_s} \tag{1}$$

where r represents the adsorbed amount of AmB (mmol/100 g), C_s is the equilibrium concentration (mmol/L), x_m is the maximum amount of adsorbed AmB (mmol/100 g) and b is the affinity constant between the AmB organic adsorbate and the MMT clay adsorbent (L/mmol). The isotherm showed a good fitting to the Langmuir model ($R^2 = 0.9998$), providing an affinity constant of 0.284 ± 0.004 L/mmol between the AmB and the clay. The values of the plateau of the adsorption isotherm correspond to a drug content of around 297 ± 2 meq per 100 g MMT. These results confirm the affinity of AmB for this smectite, which could accommodate large amounts of this antifungal drug beyond its CEC (93 meq/100 g).

The synthesis of the MMT-AmB hybrid material to be used in the further delivery study was carried out by mixing 200 mmol of AmB per 100 g of MMT, as indicated in the Experimental Section. From the adsorption isotherm, in these conditions the amount of adsorbed AmB is close to the CEC of the smectite, ensuring that the AmB are intercalated in MMT, with no excess of drug adsorbed on the external surface. The intercalation of AmB into the interlayer space of MMT is confirmed from the XRD pattern (Fig. 3A), which clearly shows a shift in the position of the peak ascribed to the $(0\ 0\ 1)$ reflection plane towards lower 2θ angles. This (0 0 1) reflection appears at 4.15° 20, corresponding to a d-value or basal space of 2.13 nm, higher than that of 1.20 nm of the starting MMT clay. Using this first reflection and other (0 0 l) rational orders, such as $(0\ 0\ 2)$ and $(0\ 0\ 4)$ reflections at 7.88° and $18.61^{\circ}\ 2\theta$, with basal space 1.12 nm and 0.48 nm, respectively, it is possible to determine a mean basal space value of 2.10 nm. Given that the thickness of a MMT single layer is approximately of 0.96 nm (Moore and Reynolds, 1989), an interlayer space of 1.14 nm was deduced for the MMT-AmB hybrid due to AmB intercalation. Considering these values and the dimensions of the amphotericin B ions estimated from ChemDraw® software from PerkinElmer, a schematic model on the possible accommodation of the drug in the interlayer space of the MMT can be proposed (Fig. 3B). According to the results of chemical analysis (Table S1), the obtained hybrid presents an AmB content of 63.5 mmol per 100 g of MMT (40.0

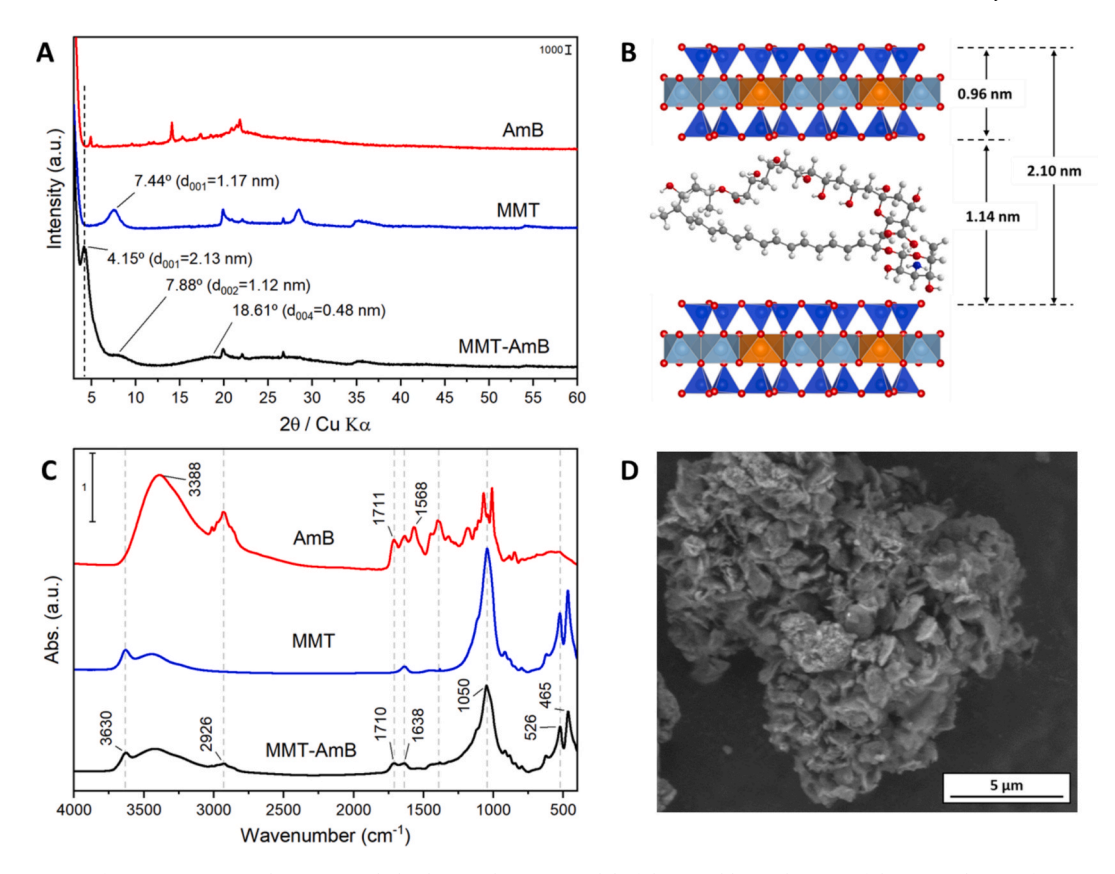


Fig. 3. (A) XRD patterns of AmB, Na-MMT and MMT-AmB hybrid; (B) Schematic model of the possible mechanism of the intercalation of AmB into Na-MMT and its accommodation between the silicate layers (Please note that this schematic representation of the hybrid does not represent the real conformation of the molecules in the interlayer space); (C) FT-IR spectra in the 4000–400 cm⁻¹ region of AmB, Na-MMT and MMT-AmB hybrid; and (D) FESEM image of the MMT-AmB hybrid.

mmol / 100 g of hybrid), which is lower than the CEC of Na-MMT (about 93 meq per 100 g of MMT). This fact could be due to the large size of this molecule, which would prevent the positively charged AmB molecules from compensating all the negatively charged sites at the MMT layers. This fact suggests that part of the surface negative charges should remain compensated with sodium ions, as confirmed by EDX results, which shows a decrease of the Na/Si ratio from 0.082 in the MMT to 0.025 in the hybrid material.

The formation of the MMT-AmB hybrid could be also confirmed by FTIR spectroscopy. The infrared spectrum of amphotericin B recorded in Fig. 3C shows the characteristic bands of this antifungal, in accordance with those reported by Gagos and Arczewska (2010). The spectrum shows a broad band centered at 3388 ${\rm cm}^{-1}$ related to ν_{O-H} and ν_{N-H} vibration modes and bands located at 1711 and 1568 cm⁻¹ that are ascribed to asymmetric stretching vibration mode of -COO⁻ group and symmetric bending in plane vibration mode of -NH₃ group, respectively (Gagoś and Arczewska, 2010). The spectrum of Na-MMT clay (Fig. 3C) shows the typical vibration bands of the silicate (Rebitski et al., 2018), with a vibration band attributed to water bending at approximately 1638 cm⁻¹, due to water directly coordinated to the exchangeable cations of the clay. This band can be also observed in the spectrum of MMT-AmB hybrid probably due to the presence of hydrated sodium cations still present in the interlayer space. The hybrid spectrum also presents most of the bands related to the vibration modes of amphotericin B. However, the absence of the band centered at $1568~\mathrm{cm}^{-1}$ indicated that the AmB could be bonded to the silicate layer by electrostatic interactions involving the -NH₃ groups, thus perturbing their bending vibration. Fig. 3D shows the morphology of the MMT-AmB hybrid observed by FESEM, where the aggregation of particles smaller than 1 µm with a layered morphology can be seen, which indicates that the morphology of the layered clay is preserved.

3.2. Synthesis and characterization of the LDH ZnAl-AmB hybrid system

The precipitation of Zn and Al to produce a Zn,Al LDH, with a molar ratio 2:1, in the presence of AmB, following the procedure detailed in the Experimental Section, led to the formation of a yellow solid (LDH ZnAl-AmB). The X-ray diffractogram of the resulting material is shown in Fig. 4A together with that of a Zn,Al LDH prepared in the absence of AmB (LDH ZnAl). The diffractogram of LDH ZnAl-AmB shows that the typical 003 reflection was shifted towards a lower (20) angle of 2.69° (Fig. S3), confirming the intercalation of AmB. In addition, several orders of reflection corresponding to planes (0 0 6), (0 0 9), (0 0 1 2), (0 0 15) and (0018) are clearly observed in the diffractogram, suggesting a good order in the stacking of LDH layers in presence of intercalated AmB molecules. From these values, a basal spacing of 3.56 nm was determined, which corresponded to an interlayer space of 3.14 nm, taking into account the thickness of brucite-like layers (0.48 nm). Such a large distance, larger than that found for MMT-AmB, would suggest the accommodation of the AmB molecules as multilayers or adopting a vertical conformation, considering the estimated dimensions of this molecule (Fig. 4B). However, theoretical calculations would be required to ascertain the real configuration in the interlayer space of both clays, what is beyond the focus of the current study.

The content of AmB in this material was determined by CHNS elemental chemical analysis, resulting in 92.2 mmol per 100 g LDH (49.8 mmol per 100 g of hybrid) (Table S1). This value is around three times lower than the AEC of this type of solid. This fact could be due to the large size of AmB, which impedes that many of the positively charged sites in the solid film could be compensated by anionic AmB molecules, similarly as mentioned above for the intercalation of AmB in MMT. As a consequence, part of the cationic sites should remain compensated by nitrate anions. Nevertheless, the coprecipitation procedure carried out in the current work led to the adsorption of a

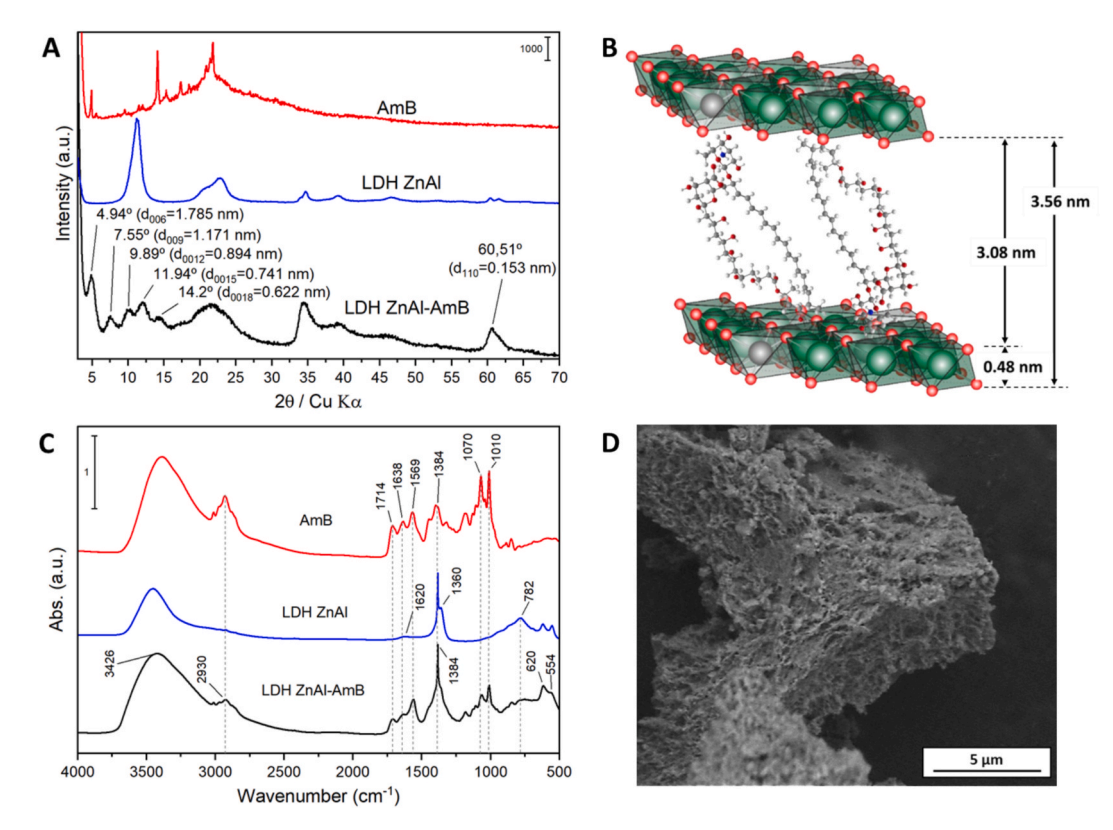


Fig. 4. (A) XRD patterns of Zn,Al LDH, with molar ratio 2:1, prepared in the absence (LDH ZnAl) or in the presence of AmB (LDH ZnAl-AmB). (B) Suggested arrangement of AmB molecules intercalated into between the LDH layers (Please note that this schematic representation of the hybrid does not represent the real conformation of the molecules in the interlayer space). (C) FTIR spectra in the 4000–500 cm⁻¹ region of AmB, LDH ZnAl and the hybrid material LDH ZnAl-AmB. (D) FESEM image of LDH ZnAl-AmB.

considerable amount of AmB (49.8 % w/w), higher than that obtained in a previous study that reported the intercalation of AmB in a Mg,Al LDH by an ion-exchange mechanism (Trikeriotis and Ghanotakis, 2007). In this last case, despite surfactants were used as coadsorbent to overcome the low solubility of AmB in aqueous media, the adsorption of AmB reached lower values in the final hybrids, below 10 % w/w. For comparison, in the present study a LDH ZnAl-AmB hybrid was also prepared in the presence of a non-ionic surfactant as coadsorbent (Triton X-100) during coprecipitation, resulting also in an intercalation material with a similar XRD pattern (Fig. S4) but with AmB content around 33 % w/w due to the presence of coadsorbed surfactant molecules. Based on the obtained results, the sample prepared by coprecipitation of the LDH in the presence of AmB without surfactant was selected for further release studies.

The FTIR spectrum of the hybrid material LDH ZnAl-AmB (Fig. 4C) shows the characteristic bands due to AmB, detailed in the previous section, together with those ascribed to the layered hydroxide. Thus, the broad band appearing at 3426 cm⁻¹ results from the overlapping of those due to ν_{O-H} and ν_{N-H} vibration modes from AmB and to the stretching vibration ν_{O-H} of water molecules and OH groups of brucite layers. The other bands attributed to AmB and detailed in the previous section, appear in the spectrum of LDH ZnAl-AmB with no appreciable shift in frequency, being those at 1638 and 1384 cm⁻¹ overlapped with those observed at 1620 and 1384 cm⁻¹ in the spectrum of pristine LDH ZnAl, attributed to the δ_{H-O-H} vibration bands and to the ν_{N-O} stretching mode of the nitrate anion, respectively. In addition, the band at 1384 cm⁻¹ in the spectrum of pristine LDH ZnAl may have a contribution from intercalated carbonate anions (asymmetric ν_{C-O} stretching mode) whose presence is suggested by XRD from the asymmetry observed in the (0 0 3) reflection. In addition, the spectrum of the hybrid material also shows bands at 782 and 620 cm⁻¹ ascribed to metal-oxygen stretching vibration modes, and at 554 cm $^{-1}$ attributed to $\delta_{\text{O-M-O}}$ vibration mode in the brucite layers.

The morphology of the hybrid material LDH ZnAl-AmB was evaluated by FESEM (Fig. 4D). The image shows the presence of small layered particles agglomerated in a very compact material, which differs from the typical LDH morphology resembling of agglomerated particles with a desert rose organization. This feature could be most likely due to a strong interaction and more compact organization of the inorganic layers when formed in the presence of the organic AmB molecules.

3.3. Stability of AmB intercalated in MMT and LDH

The use of AmB is limited due to the severe side effects produced after its parenteral administration, which some authors attribute to the aggregation of AmB as dimers or tetramers (Gagoś et al., 2008; Wasko et al., 2012; Yu et al., 2022), while others suggest the possibility that toxicity may be caused by the presence of oxidized forms of AmB (Gagos and Czernel, 2014; Klimek et al., 2016). When AmB is present in HCl (0.2 M)/MeOH 50 % solution as monomers (Fig. S5), three absorbance maxima are clearly observed at around 365, 385 and 408 nm (Sawangchan et al., 2023), being this last wavelength the one usually selected to prepare a calibration curve. However, at neutral pH or in solvents where AmB solubility is low, AmB aggregates are formed, leading to the decrease of those bands and the increase of the one centered at 345 nm (Fig. S5), being the aggregation confirmed when the A₃₄₅/A₄₀₈ ratio is higher than 2 (Yu et al., 2022). In other cases, a new set of bands appears at wavelengths of around 286, 306, 321, 335 and 353 nm (Fig. S5) in agreement with results reporting the oxidation of AmB (Gagoś and Czernel, 2014). When MMT-AmB or LDH ZnAl-AmB are dispersed in aqueous media, the released molecules that remain long time in the aqueous medium can undergo these processes of aggregation and oxidation, as confirmed from their UV-vis spectra (Fig. 5). The AmB molecules remaining in solution evolve with a progressive

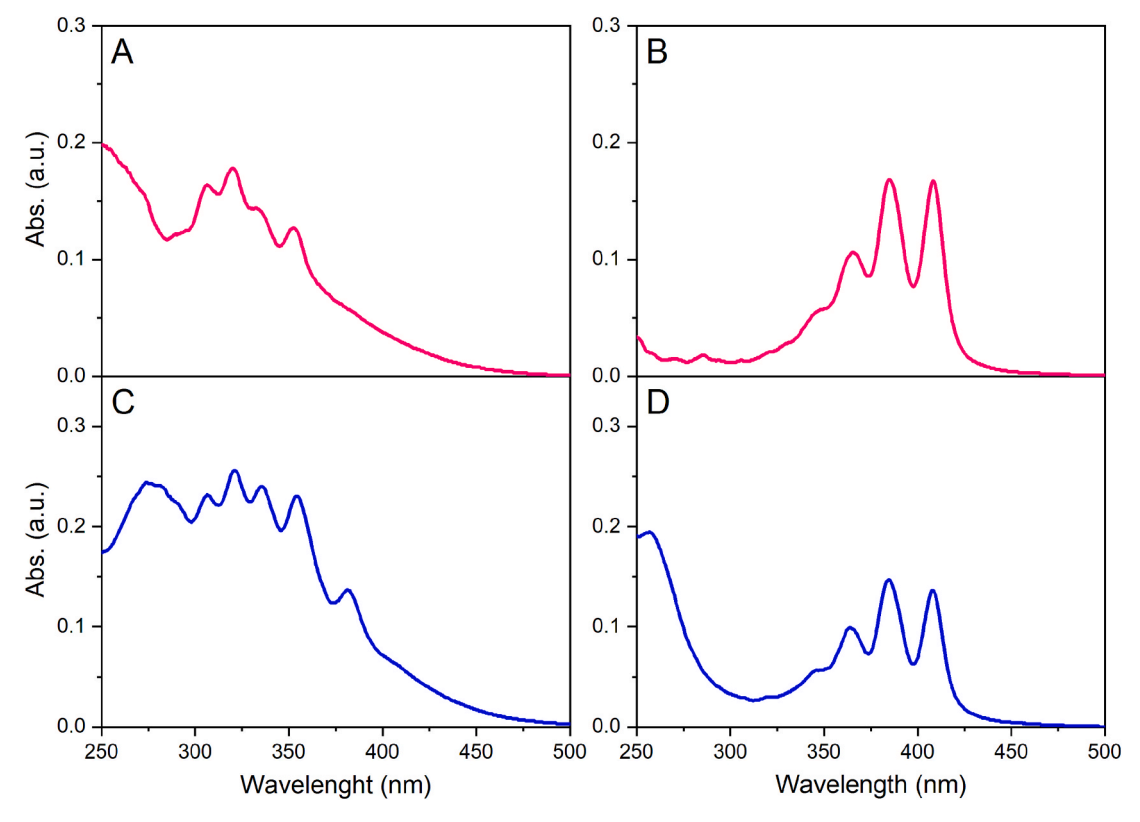


Fig. 5. UV—vis spectra of (A) AmB released from LDH ZnAl-AmB hybrid in aqueous SDB for 2 days and (B) AmB extracted by dissolving the LDH ZnAl-AmB hybrid recovered after the release experiment in (A); (C) AmB released from MMT-AmB hybrid in aqueous SDB for 2 days and (D) AmB extracted from the same MMT hybrid recovered after the release experiment in (C). In these cases, the recovered solid was dissolved or extracted with DMSO/HCl (0.2 M) 80:20 and the spectra of the obtained AmB were recorded after dilution in HCl (0.2 M)/MeOH 50 %, 1:5 for (A and C) and 1:50 for (B and D).

Table 1Comparison of AmB degradation peak temperatures in each hybrid material.

Sample	1st peak	2nd peak	3rd peak
AmB	190 °C	326 °C	479 °C
MMT-AmB	_	336 °C	626 °C
LDH ZnAl-AmB	_	309 °C	489 °C

oxidation as elapsed time increases. In contrast, the inorganic layers can offer protection to the intercalated molecules preventing them from decomposition processes. This fact was demonstrated by recovering the solids from the release medium after long periods and dissolving the inorganic layers of Zn,Al LDH with DMSO/HCl or by extraction of the AmB molecules with DMSO/HCl in the case of MMT-AmB. In both cases the extracted molecules appeared as monomers, with no oxidized form present (Fig. 5), confirming the protective role of these layered materials to guarantee the stability of intercalated AmB.

In addition, the intercalation of organic molecules in layered inorganic solid typically contributes to enhance their thermal stability, as the inorganic layers can delay the decomposition processes, as reported for many entrapped organic compounds, including drug molecules (García-Vázquez et al., 2020; Gilman, 1999; Ribeiro et al., 2014). The TG and DTA curves of AmB and the hybrid materials (Fig. S6) show that the mass loss appearing between around 200 and 600 °C, attributed to the decomposition of AmB, is associated with three exothermic processes at 190, 326 and 479 °C for pure AmB. In contrast, the DTA curve for the MMT-AmB hybrid shows only two exothermic peaks, shifted to higher temperature at 336 and 626 °C, appearing before the endothermic peak around 700 °C attributed to the dehydroxylation process of MMT (Ge et al., 2024). This delay in the exothermic peaks, together with the continued weight loss in this temperature range, would confirm the

Table 2First mass loss and residue percentages of the hybrid and pristine materials calculated from TG curves and the estimated AmB mass percentage in the hybrid material.

Water mass loss (%)	Residue (%)	AmB content (%)
7.4	87.4	_
6.0	58.4	33.2
2.2	68.4	_
7.3	33.2	51.5
	7.4 6.0 2.2	7.4 87.4 6.0 58.4 2.2 68.4

protective effect exerted by the silicate layers, which leads to the retention of degradation products within the silicate layers. Similarly, the DTA curve of LDH ZnAl-AmB hybrid shows two exothermic peaks at 309 °C and 489 °C, the last one presenting a slight delay with respect to pure AmB, which could confirm again the protection of the LDH layers. Table 1 summarizes the temperatures of the AmB degradation peaks for each hybrid system. The first degradation peak of AmB is not clearly distinguishable in any of the hybrid materials. This absence is likely attributed to strong interactions between AmB and the inorganic host layers, which may stabilize its more labile functional groups and restrict molecular mobility. As a result, the initial decomposition pathways are hindered, leading to the suppression or displacement of the corresponding thermal event and rendering the first degradation step undetectable under the applied conditions. The enhanced thermal stability conferred by the layered structures is evidenced by the shift of the third degradation peak to higher temperatures, with the most pronounced protective effect observed in the MMT-based hybrid.

All TG curves of the hybrid and pristine materials exhibit an initial mass loss up to approximately 150 $^{\circ}$ C, which is associated with the removal of physisorbed water. This water mass loss (Table 2) provides valuable information about the hydrophilicity and water retention

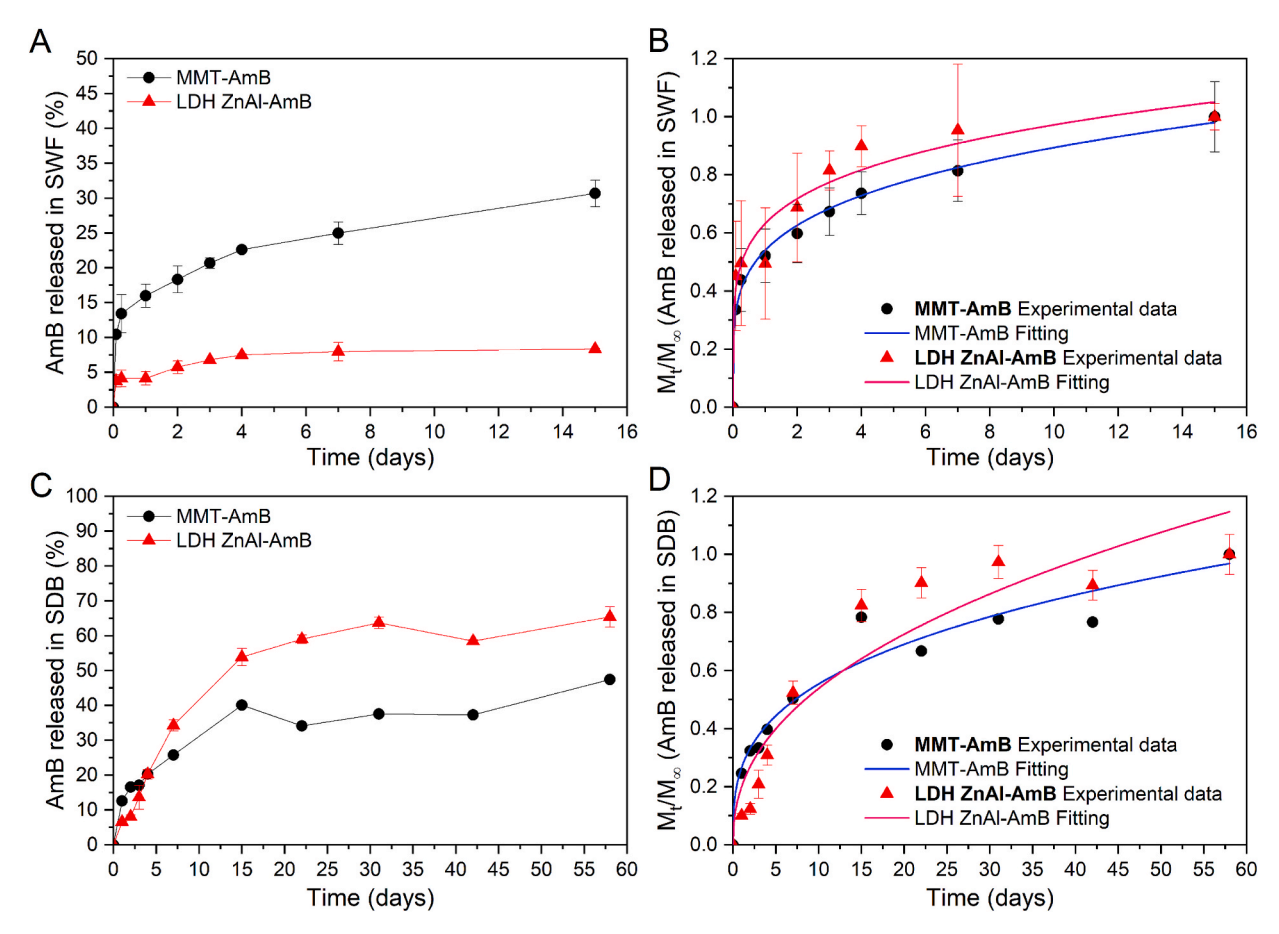


Fig. 6. Percentage of AmB released from MMT-AmB and LDH ZnAl-AmB hybrids in SWF (A) and in SDB (C) media, and Peppas-Sahlin fitting to the release experimental data in SWF (B) and in SDB (D) media.

behavior of the materials. Pristine MMT shows a higher water loss (7.4 %) than the MMT–AmB hybrid (6.0 %), indicating that the incorpoartion of AmB partially removes interlayer water. In contrast, LDH ZnAl displays a much lower water loss (2.2 %), which can be attributed to the fact that water in LDH structures is more strongly coordinated within the interlayered space, requiring higher temperatures for its release. However, the LDH ZnAl-AmB hybrid shows a significantly higher water loss (7.3 %), suggesting again that the incorporation of AmB alters the interlayer environment and facilitates the loss of water from the LDH at lower temperature.

Furthermore, considering that both MMT and LDH are inorganic materials, they exhibit a high residual mass after calcination, whereas AmB, being an organic compound, is completely decomposed under these conditions (Fig. S6). From the TG curves, it is possible to calculate the residual mass of both the pristine and hybrid materials, allowing estimation of the AmB content in the hybrids using the rule of mixtures.

$$R_h = w_{clay} \cdot R_{clay} + w_{AmB} \cdot R_{AmB}$$
 (2)

where w_{clay} and w_{AmB} are the mass fraction in the hybrid of the clay material (MMT or LDH ZnAl) and the AmB, respectively; and R_h , R_{clay} and R_{AmB} are the residual mass of the hybrid material, the clay material (MMT or LDH ZnAl) and the AmB, respectively. Given that R_{AmB} is 0 % (Fig. S6), the Eq. (2) can be simplified and the fraction mass of the clay component and the AmB content can be calculated:

$$w_{\text{clay}} = \frac{R_h}{R_{\text{clay}}} \tag{3}$$

$$w_{AmB} = 1 - w_{clay} \tag{4}$$

The estimated AmB contents for the hybrid materials are $33.2\,\%$ and $51.5\,\%$, which are in good agreement with the values obtained from elemental chemical analysis. Specifically, the AmB content in the MMT–AmB hybrid was determined to be $37\,\mathrm{g}$ per $100\,\mathrm{g}$ of hybrid, while in the LDH ZnAl-AmB hybrid was 46 g per $100\,\mathrm{g}$ of hybrid. The discrepancy in mass loss values between these two methods can be attributed to the loss of water molecules hosted within the interlayer spaces, as well as the possible presence of other species, such as nitrate or carbonate anions, in the interlayer space of the LDH, or pyrolyzed species in MMT.

3.4. In vitro release of AmB from MMT-AmB and LDH ZnAl-AmB hybrids

The release of AmB from both hybrid materials was carried out in a SWF medium consisting of NaCl and CaCl₂, as well as in SDB medium, in which the *in vitro* studies of antifungal activity were further performed, as detailed in the Experimental Section. The amount of released AmB from MMT-AmB and LDH ZnAl-AmB hybrid materials was determined by UV–vis spectrophotometry (Fig. S7). In SWF, a fast release of AmB is observed in both cases within the first hours, and the release rate is then reduced in the following days (Fig. 6). MMT-AmB presents a delivered amount of around 30.7 % of the encapsulated AmB after 15 days. In contrast, the release kinetics from LDH ZnAl-AmB are slower during the second week of the experiment, releasing only 8.4 % of AmB after the same period.

Regarding the experiments carried out in SDB, the release kinetics were faster during the first two weeks and then the release rate diminished in the next weeks. The AmB amounts delivered after 15 days reached values of 40 % and 55 % for MMT-AmB and LDH ZnAl-AmB, respectively, which are higher than those obtained in the previous

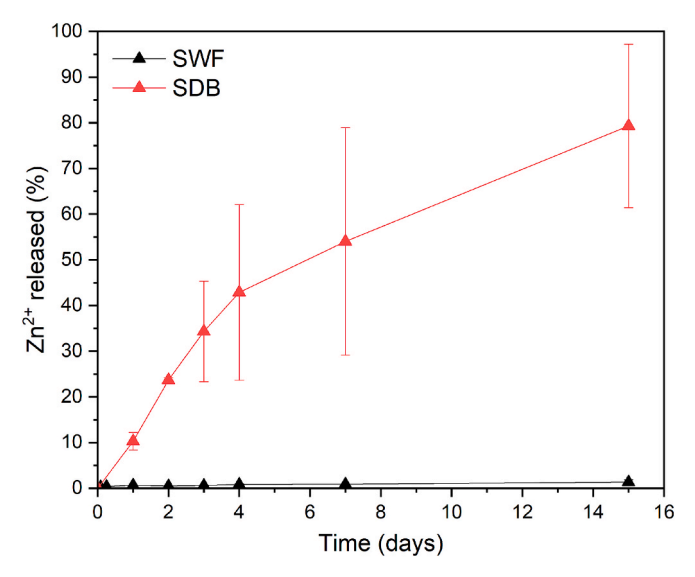


Fig. 7. Percentage of Zn^{2+} released from the LDH ZnAl-AmB hybrid in SWF and in SDB media.

experiment in SWF after the same period. This difference could be attributed to components in SDB such as peptone (protein hydrolysates) with higher affinity for both MMT and LDH than the NaCl and CaCl₂ salts present in SWF. A similar behavior has been observed in an analogue drug release system based on Laponite-itraconazole (Jung et al., 2008), which showed an increase in the delivery rate in the presence of cationic surfactants or a cationic polymer such as Eudragit® E-100 in the release medium compared to that in NaCl solution. Regarding the LDH hybrid material, the release of AmB is much higher in SDB, overpassing that of MMT-AmB. This fact could be also due to the slow dissolution of this last solid in aqueous media, showing a gradual release of Zn²⁺ cations as determined by TXRF, which is faster in the SDB medium most likely due to the interaction with the SDB components (Fig. 7). The release of AmB in SDB was evaluated up to almost 2 months, reaching values of 47 % and 65 % for MMT-AmB and LDH ZnAl-AmB, respectively, which would guarantee the performance of these materials as a reservoir of AmB for possible in vivo use where a long-term treatment is required.

The release profile of AmB from the hybrid materials was evaluated using four kinetic models: Korsmeyer–Peppas, Peppas–Burst, Peppas–Sahlin, and Weibull (Fig. S8) (Bruschi, 2015; Peppas and Narasimhan, 2014). Among them, the Peppas–Sahlin model provided the best overall fit across the full experimental time range, as evidenced by its higher coefficient of determination (R^2), in the range of 0.90 to 0.99, and lower root mean square error (*RMSE*), in comparison with other kinetic models (Table S2).

Although the Korsmeyer-Peppas model also showed in most cases a good correlation with the experimental data, its application is limited to the initial 60 % of the release, and does not adequately describe the later stages (Ritger and Peppas, 1987a, 1987b). The Peppas-Burst model also provided acceptable fits. However, the very low value of the burst parameter (*B*) suggests a negligible initial burst effect, which makes this model less representative of the system. Based on these results, Peppas-Burst model was not even applied to the release data in the SDB medium.

Alternatively, Peppas–Sahlin model allows the distinction between the Fickian diffusion and relaxation (non-Fickian) mechanisms, making it suitable for describing the entire release profile. This is particularly relevant in hybrid systems where both diffusion through the matrix and structural relaxation of the carrier may contribute, especially at later stages of release (Peppas and Sahlin, 1989). Consequently, the relative magnitudes of k_1 , k_2 , and m in Eq. S3 provide insight into the dominant mechanisms controlling drug release in a given formulation.

Table 3Parameters and statistical metrics of the Peppas-Sahlin fitting model to the AmB release curve of each hybrid material in the two release media studied.

Sample	Release	Parameters	Parameters			RMSE
	media	k_1 [day ^{-m}]	k_2 [day ^{-2m}]	m		
MMT- AmB	SWF	0.37 ± 6.88	0.17 ± 6.87	0.16 ± 1.55	0.9954	0.0228
LDH ZnAl-	SWF	$\begin{array}{c} \textbf{0.31} \pm \\ \textbf{3.70} \end{array}$	$\begin{array}{c} 0.32 \pm \\ 3.71 \end{array}$	$\begin{array}{c} 0.12 \\ \pm \ 0.46 \end{array}$	0.9572	0.0762
AmB MMT- AmB	SDB	$\begin{array}{c} \textbf{0.27} \pm \\ \textbf{0.05} \end{array}$	$\begin{array}{c} 0.00 \pm \\ 0.08 \end{array}$	$\begin{array}{c} 0.32 \\ \pm \ 0.22 \end{array}$	0.9535	0.0716
LDH ZnAl- AmB	SDB	$\begin{array}{c} 0.20 \; \pm \\ 0.05 \end{array}$	$\begin{array}{c} 0.00 \pm \\ 0.05 \end{array}$	$\begin{array}{l} 0.43 \\ \pm \ 0.33 \end{array}$	0.9055	0.1356

Based on the considerations of the different models, the Peppas-Sahlin model was selected as the most suitable to describe the AmB release behavior in the hybrid systems studied. As shown in Table 3, the best fit was obtained for the MMT-AmB system in SWF, with a high R^2 value of 0.9954 and a low RMSE of 0.0228, indicating excellent agreement with the experimental data. For the LDH ZnAl-AmB hybrid in the same medium, the model continued to show a good fit ($R^2 = 0.9572$; RMSE = 0.0762), although slightly less accurate than for MMT-AmB. In the SDB medium, the fitting goodness decreased for both materials, particularly in release using the LDH ZnAl-AmB hybrid ($R^2 = 0.9055$; RMSE = 0.1356), reflecting the different interaction between the hybrid materials and the components of the release medium, such as metioned above.

The values of the exponent m in the Peppas–Sahlin model ranged from 0.12 to 0.43 across the different systems, indicating that the release mechanism was predominantly Fickian in nature. Additionally, the higher standard errors associated with m in some cases may reflect experimental variability or overlapping contributions from diffusion and matrix relaxation.

Notably, the parameter k_2 , associated with the relaxation contribution (non-Fickian), was close to zero for both hybrid materials using the SDB release medium, suggesting a predominantly Fickian release in this medium. These results further support the suitability of the Peppas-Sahlin model, especially under SWF conditions, where both diffusion and matrix relaxation contribute to the release process.

On the other hand, although the Weibull model offers empirical flexibility, it lacks a mechanistic interpretation of the underlying release phenomena. Nevertheless, it provided reasonably good fits for all systems, with R^2 values ranging from 0.93 to 0.99 (Table S2). In SWF, both MMT–AmB and LDH ZnAl–AmB exhibited β values below 0.4, indicative of an initial burst followed by a decelerated release phase, consistent with diffusion-controlled mechanisms. In SDB medium, MMT–AmB maintained a $\beta<1$ (0.54), suggesting a sustained release with moderate burst, while LDH ZnAl–AmB showed a $\beta>1$ (1.10), implying a different release profile possibly influenced by stronger drug–matrix interactions. Additionally, the α values, which are associated with the time scale of the release process, were higher in SDB, indicating a slower release compared to SWF.

After the release experiments, the remaining solids were recovered and observed again by FESEM. The release of AmB increases the porosity in both hybrid materials (Fig. S9).

3.5. Evaluation of antifungal activity against eumycetoma causative

The performance of MMT-AmB and LDH ZnAl-AmB hybrids was evaluated *in vitro* against fungal strains of *Aspergillus flavus* and *Sub-ramaniula thielavioides*, isolated from human eumycetoma cases from Turkana County in Northwestern Kenya (Colom et al., 2023). Both AmB

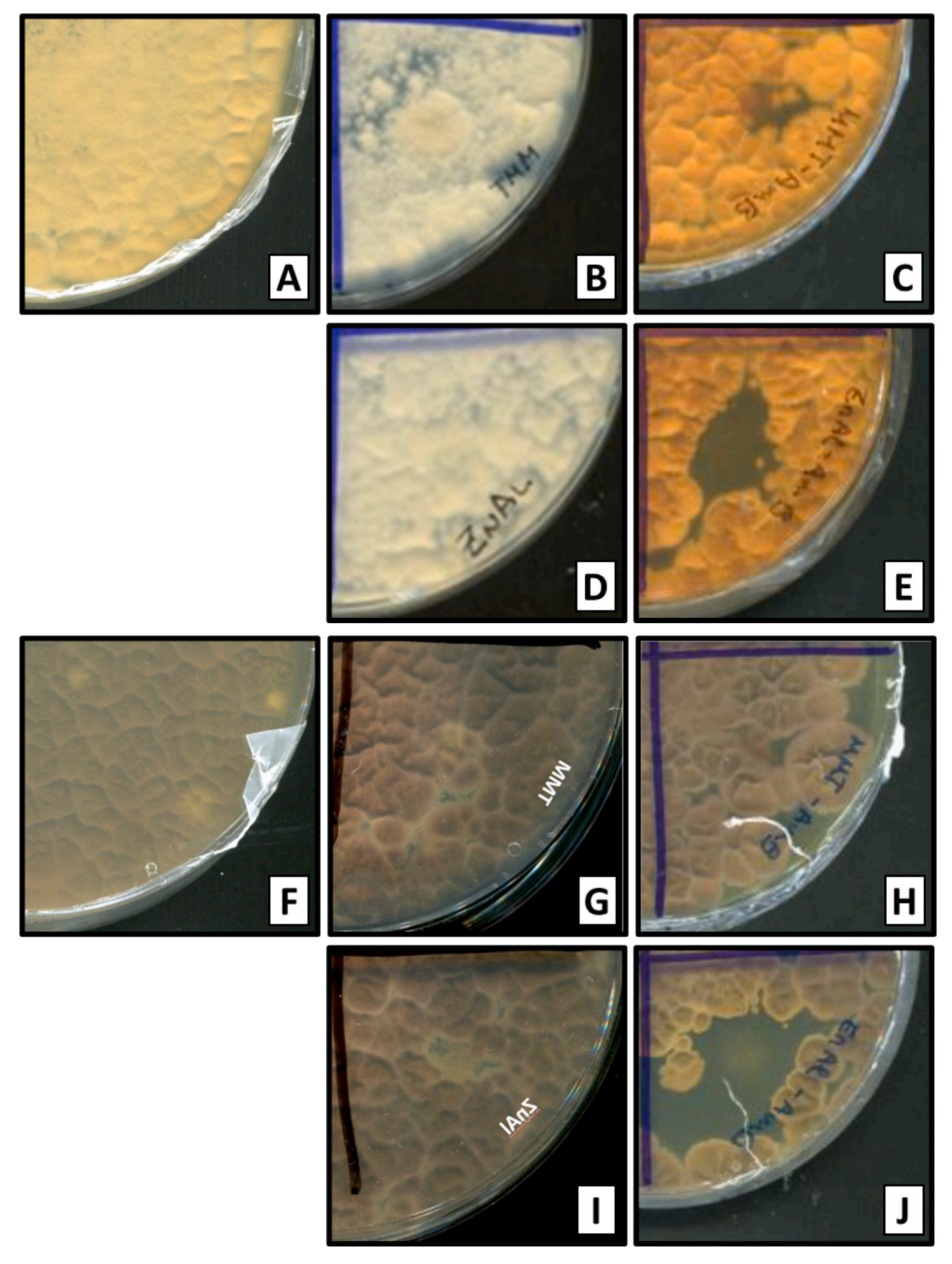


Fig. 8. Control growth of Aspergillus flavus on a plate with solid SDB medium (A), negative growth control in the presence of (B) Na-MMT or (D) LDH ZnAl and growth inhibition in the areas where (C) MMT-AmB or (E) LDH ZnAl-AmB were deposited. Control growth of Subramaniula thielavioides on a plate with solid SDB medium (F), negative growth control in the presence of (G) Na-MMT or (I) LDH ZnAl and growth inhibition in the areas where (H) MMT-AmB or (J) LDH ZnAl-AmB were deposited.

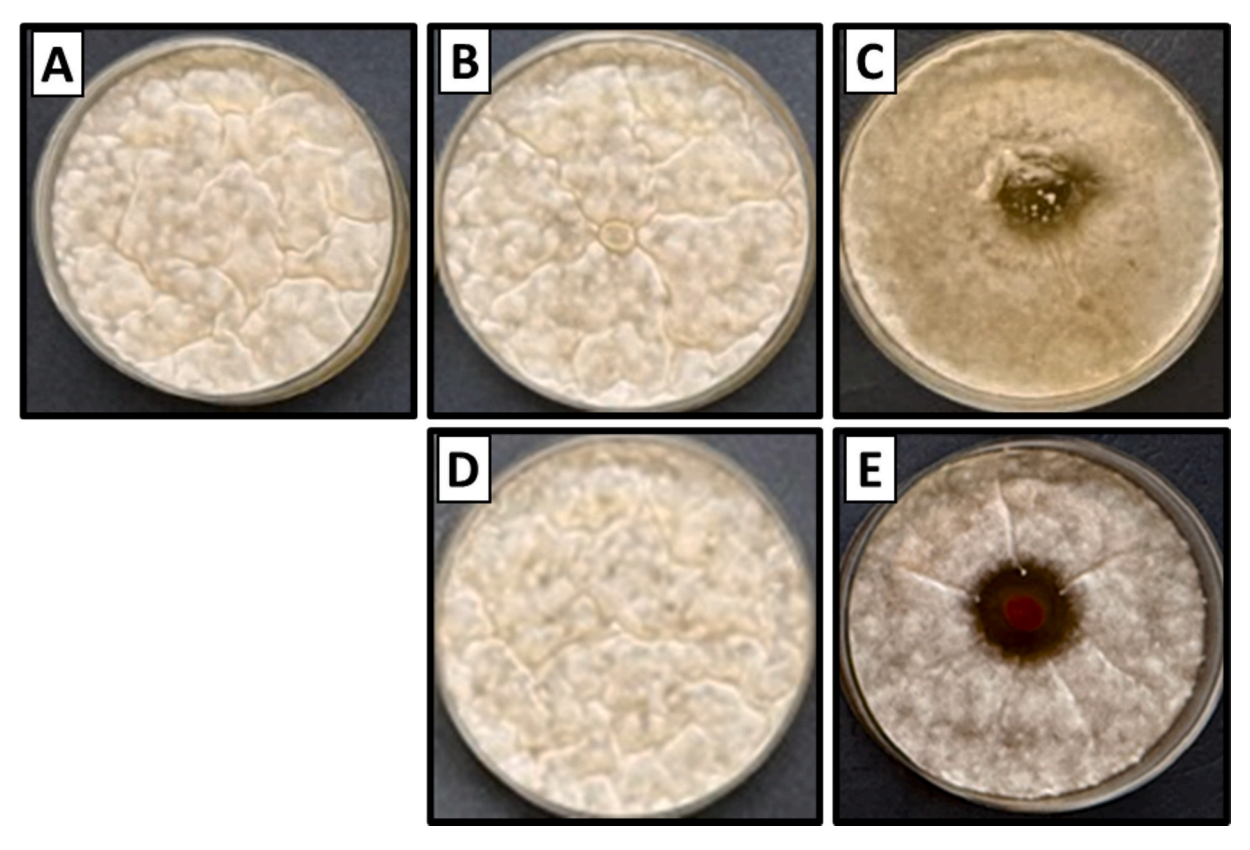


Fig. 9. Control growth of *A. flavus* on a plate with semi-solid BHI medium (A), negative growth control in the presence of (B) Na-MMT or (D) LDH ZnAl and growth inhibition in the areas where (C) MMT-AmB or (E) LDH ZnAl-AmB were deposited.

hybrids showed growth inhibition in both species tested. A sustained release of the drug over time could be observed for both tested hybrid materials, as the inhibition halos against the fungus are maintained seven days after inoculation.

In accordance with the release studies carried out in SDB medium, which confirmed a gradual release of the drug over 15 days of study, inhibition tests were carried out in a similar composition medium. On solid SDA medium, it was observed that in both fungal species tested, the LDH ZnAl-AmB hybrid (Fig. 8E and J) generates a greater inhibition than the MMT-AmB hybrid (Fig. 8C and H). Subsequently, aiming at testing the developed materials in a medium with a texture more similar to the subcutaneous fungal masses, experiments were carried out on semi-solid medium with BHI at 1.5 % agar. The most stable results were obtained with A. flavus, which showed an important inhibition of growth in the presence of both hybrid formulations, although it was more evident with LDH ZnAl-AmB than with MMT-AmB (Fig. 9), as observed in the SDA tests. Since S. thielavioides does not sporulate like A. flavus, in the semi-solid BHI medium, the lawn form of this fungus is not easily achieved, which makes it difficult to test the hybrid materials to observe their inhibitory effect. However, the tests performed suggested an inhibitory effect slightly more pronounced with MMT-AmB. In general, S. thielavioides seems to have a minor sensitivity, although with both species tested the inhibitory effect of the prepared hybrid materials can be observed. The administration of these AmB release systems, once formulated in hydrogels, is foreseen for local injection by ultrasoundguided puncture into the mycetoma lesion. The obtained results show that the developed hybrid materials are promising for the treatment of eumycetoma and their performance will be optimized in further studies.

4. Concluding remarks

Montmorillonite (MMT), showing cation exchange capacity, and Zn, Al layered double hydroxide (LDH), with anion exchange capacity, were

evaluated as supports for the intercalation of the antifungal drug amphotericin B (AmB), taking advantage of its amphoteric character. The resulting hybrid materials contain large amounts of AmB, 63.5 mmol per 100 g of MMT and 92.2 mmol per 100 g of LDH, respectively, overpassing those reported in related systems. The inorganic solids encapsulated AmB protecting it against aggregation and oxidation in aqueous media, which according to several reports can be responsible for the toxic effects of AmB. The antifungal release study carried out in a simulated wound fluid (SWF) and in the Sabouraud Dextrose Broth (SDB) growth medium confirms a sustained release of AmB from the different supports, confirming the usefulness of these systems for applications in long-term antifungal treatments. Furthermore, in vitro tests of the different hybrid materials were carried out against two causative agents of eumycetoma, Aspergillus flavus and Subramaniula thielavioides, confirming their capacity to inhibit the fungus growth. This preliminary result shows the potential of AmB intercalated in layered clays for the treatment of eumycetoma. Further studies will be carried out to optimize these antifungal systems and explore their application to treat other fungal infections.

CRediT authorship contribution statement

Alexander Misol: Writing – review & editing, Writing – original draft, Validation, Methodology, Investigation, Formal analysis, Data curation. Esther Sáez: Writing – original draft, Methodology, Investigation, Formal analysis, Data curation. María Francisca Colom: Writing – review & editing, Writing – original draft, Supervision, Methodology, Funding acquisition, Formal analysis, Data curation, Conceptualization. Margarita Darder: Writing – review & editing, Writing – original draft, Supervision, Methodology, Investigation, Funding acquisition, Formal analysis, Data curation, Conceptualization. Pilar Aranda: Writing – review & editing, Supervision, Project administration, Methodology, Funding acquisition, Formal analysis, Data

curation, Conceptualization.

Declaration of competing interest

The authors declare that they have no known competing financial interests or personal relationships that could have appeared to influence the work reported in this paper.

Acknowledgements

The authors acknowledge the Severo Ochoa Centres of Excellence program through Grant CEX2024-001445-S and the Agencia Estatal de Investigación, MCIN/AEI/10.13039/501100011033 (Spain, projects PID2019-105479RB-I00 and PID2022-137889OB-I00) and "ERDF A way of making Europe" (EU, project PID2022-137889OB-I00), as well as partial financial support by a grant for research projects linked to international development cooperation UMH-GVA (Spain), reference SOLCIF 2022/0005 (COD. 11-134-4-2023-0133).

Appendix A. Supplementary data

Supplementary data to this article can be found online at https://doi.org/10.1016/j.ijpharm.2025.126029.

Data availability

Data will be made available on request.

References

- Aguzzi, C., Cerezo, P., Viseras, C., Caramella, C., 2007. Use of clays as drug delivery systems: possibilities and limitations. Appl. Clay Sci. 36, 22–36. https://doi.org/ 10.1016/j.clay.2006.06.015
- Ahmed, A.O., van Leeuwen, W., Fahal, A., van de Sande, W., Verbrugh, H., van Belkum, A., 2004a. Mycetoma caused by Madurella mycetomatis: a neglected infectious burden. Lancet Infect. Dis. 4, 566–574. https://doi.org/10.1016/S1473-3099(04)01131-4
- Ahmed, A.O.A., De Hoog, G.S., van de Sande, W.W.J., 2015. Fungi causing Eumycotic mycetoma. In: Manual of Clinical Microbiology. ASM Press, Washington, DC, USA. pp. 2173–2187. Doi: 10.1128/9781555817381.ch125.
- Ahmed, A.O.A., van de Sande, W.W.J., van Vianen, W., van Belkum, A., Fahal, A.H., Verbrugh, H.A., Bakker-Woudenberg, I.A.J.M., 2004b. In Vitro susceptibilities of *Madurella mycetomatis* to itraconazole and amphotericin B assessed by a modified NCCLS method and a viability-based 2,3-bis(2-methoxy-4-nitro-5- sulfophenyl)-5-[(phenylamino)carbonyl]-2 *H* tetrazolium hydroxide (XTT) assay. Antimicrob. Agents Chemother. 48, 2742–2746. https://doi.org/10.1128/AAC.48.7.2742-2746.2004.
- Bruschi, M.L. (Ed.), 2015. Mathematical models of drug release. In: Strategies to Modify the Drug Release from Pharmaceutical Systems. Woodhead Publishing. pp. 63–86. Doi: 10.1016/B978-0-08-100092-2.00005-9.
- Canada, T.A., Cowan, M.E., Wiencek, K.M., 2011. Wound Care Device Having Fluid Transfer Properties (Patent No. US 8021685 B2).
- Chandler, D.J., Bonifaz, A., van de Sande, W.W.J., 2023. An update on the development of novel antifungal agents for eumycetoma. Front. Pharmacol. 14, 1165273. https:// doi.org/10.3389/fphar.2023.1165273.
- Colom, M.F., Ferrer, C., Ekai, J.L., Ferrández, D., Ramírez, L., Gómez-Sánchez, N., Leting, S., Hernández, C., 2023. First report on mycetoma in Turkana County—North-western Kenya. PLoS Negl. Trop. Dis. 17, e0011327. https://doi.org/ 10.1371/journal.pntd.0011327.
- Cui, N., Zhao, J., 2024. Application and evaluation of topical amphotericin B for the treatment of respiratory fungal infections. BMC Infect. Dis. 24, 439. https://doi.org/ 10.1186/s12879-024-09342-9.
- Dash, S.K., Benival, D., Jindal, A.B., 2024. Formulation strategies to overcome amphotericin B induced toxicity. Mol. Pharm. 21, 5392–5412. https://doi.org/ 10.1021/acs.molpharmaceut.4c00485.
- Estrada, R., Chávez-López, G., Estrada-Chávez, G., López-Martínez, R., Welsh, O., 2012. Eumycetoma. Clin. Dermatol. 30, 389–396. https://doi.org/10.1016/j.clindermatol.2011.09.009.
- CDC Mycetoma, 2024. Clinical Overview of Mycetoma [WWW Document]. URL https://www.cdc.gov/mycetoma/hcp/clinical-overview/index.html# (accessed 11 October 2024).
- EUCAST, 2011. Amphotericin B and Aspergillus spp.: Rationale for the clinical breakpoints, v1.0. https://www.eucast.org/uploads/media/AmphotericinB_Aspergi llus_consult.pdf (accessed 30 July 2025).
- Gagoś, M., Arczewska, M., 2010. Spectroscopic studies of molecular organization of antibiotic amphotericin B in monolayers and dipalmitoylphosphatidylcholine lipid

- multibilayers. Biochim. Biophys. Acta Biomembr. 1798, 2124–2130. https://doi.org/10.1016/j.bbamem.2010.07.037.
- Gagoś, M., Czernel, G., 2014. Oxidized forms of polyene antibiotic amphotericin B. Chem. Phys. Lett. 598, 5–9. https://doi.org/10.1016/j.cplett.2014.02.052.
- Gagoś, M., Hereć, M., Arczewska, M., Czernel, G., Dalla Serra, M., Gruszecki, W.I., 2008. Anomalously high aggregation level of the polyene antibiotic amphotericin B in acidic medium: implications for the biological action. Biophys. Chem. 136, 44–49. https://doi.org/10.1016/j.bpc.2008.04.005.
- Gallis, H.A., Drew, R.H., Pickard, W.W., 1990. Amphotericin B: 30 years of clinical experience. Clin. Infect. Dis. 12, 308–329. https://doi.org/10.1093/clinids/ 12.2.308.
- García-Vázquez, R., Rebitski, E.P., Viejo, L., de los Ríos, C., Darder, M., García-Frutos, E. M., 2020. Clay-based hybrids for controlled release of 7-azaindole derivatives as neuroprotective drugs in the treatment of Alzheimer's disease. Appl. Clay Sci. 189, 105541. https://doi.org/10.1016/j.clay.2020.105541.
- Ge, W., Mao, H., Chen, J., Min, F., Liu, H., Song, S., 2024. Understanding the thermal activation behavior of montmorillonite and kaolinite at atomic level by ReaxFF molecular dynamics simulations. Appl. Clay Sci. 251, 107313. https://doi.org/ 10.1016/j.clay.2024.107313
- Gilman, J., 1999. Flammability and thermal stability studies of polymer layered-silicate (clay) nanocomposites. Appl. Clay Sci. 15, 31–49. https://doi.org/10.1016/S0169-1317(99)00019-8.
- Jung, H., Kim, H.-M., Choy, Y.B., Hwang, S.-J., Choy, J.-H., 2008. Laponite-based nanohybrid for enhanced solubility and controlled release of itraconazole. Int. J. Pharm. 349, 283–290. https://doi.org/10.1016/j.ijpharm.2007.08.008.
- Klimek, K., Strubińska, J., Czernel, G., Ginalska, G., Gagoś, M., 2016. In vitro evaluation of antifungal and cytotoxic activities as also the therapeutic safety of the oxidized form of amphotericin B. Chem. Biol. Interact. 256, 47–54. https://doi.org/10.1016/ i.cbi.2016.06.022.
- Kloezen, W., Parel, F., Brüggemann, R., Asouit, K., Helvert-Van Poppel, M., Fahal, A., Mouton, J., Van De Sande, W., 2018. Amphotericin B and terbinafine but not the azoles prolong survival in Galleria mellonella larvae infected with Madurella mycetomatis. Med. Mycol. 56, 469–478. https://doi.org/10.1093/mmy/myx064.
- Kuiper, L., Ruijgrok, E.J., 2009. A review on the clinical use of inhaled amphotericin B. J. Aerosol Med. Pulm. Drug Deliv. https://doi.org/10.1089/jamp.2008.0715.
- Moore, D.M., Reynolds Jr., R.C., 1989. X-ray Diffraction and the Identification and Analysis of Clay Minerals. Oxford University Press, New York. https://doi.org/ 10.1346/CCMN.1990.0380416.
- Nahar, M., Mishra, D., Dubey, V., Jain, N.K., 2008. Development, characterization, and toxicity evaluation of amphotericin B-loaded gelatin nanoparticles. Nanomedicine 4, 252–261. https://doi.org/10.1016/j.nano.2008.03.007.
- Noor, A., Preuss, C. V., 2024. Amphotericin B, in: StatPearls [Internet]. StatPearls Publishing, Treasure Island (FL). https://www.ncbi.nlm.nih.gov/books/ NBK482327/ (accessed 30 July 2025).
- Park, H., Otte, A., Park, K., 2022. Evolution of drug delivery systems: from 1950 to 2020 and beyond. J. Control. Release 342, 53–65. https://doi.org/10.1016/j. jconrel.2021.12.030.
- Patra, J.K., Das, G., Fraceto, L.F., Campos, E.V.R., del P. Rodriguez-Torres, M., Acosta-Torres, L.S., Diaz-Torres, L.A., Grillo, R., Swamy, M.K., Sharma, S., Habtemariam, S., Shin, H.-S., 2018. Nano based drug delivery systems: recent developments and future prospects. J. Nanobiotechnol. 16, 71. https://doi.org/10.1186/s12951-018-0392-8.
- Peppas, N.A., Narasimhan, B., 2014. Mathematical models in drug delivery: how modeling has shaped the way we design new drug delivery systems. J. Control. Release 190, 75–81. https://doi.org/10.1016/j.jconrel.2014.06.041.
- Peppas, N.A., Sahlin, J.J., 1989. A simple equation for the description of solute release. III. Coupling of diffusion and relaxation. Int. J. Pharm. 57, 169–172. https://doi.org/10.1016/0378-5173(89)90306-2.
- Rebitski, E.P., Aranda, P., Darder, M., Carraro, R., Ruiz-Hitzky, E., 2018. Intercalation of metformin into montmorillonite. Dalton Trans. 47, 3185–3192. https://doi.org/10.1039/c7dt04197g.
- Ribeiro, L.N.M., Alcântara, A.C.S., Darder, M., Aranda, P., Herrmann, P.S.P., Araújo-Moreira, F.M., García-Hernández, M., Ruiz-Hitzky, E., 2014. Bionanocomposites containing magnetic graphite as potential systems for drug delivery. Int. J. Pharm. 477, 553–563. https://doi.org/10.1016/j.ijpharm.2014.10.033.
- Ritger, P.L., Peppas, N.A., 1987a. A simple equation for description of solute release I. Fickian and non-fickian release from non-swellable devices in the form of slabs, spheres, cylinders or discs. J. Control. Release 5, 23–36. https://doi.org/10.1016/ 0168-3659(87)90034-4.
- Ritger, P.L., Peppas, N.A., 1987b. A simple equation for description of solute release II. Fickian and anomalous release from swellable devices. J. Control. Release 5, 37–42. https://doi.org/10.1016/0168-3659(87)90035-6.
- Rives, V., 2001. Layered Double Hydroxides: Present and Future. NOVA Science Publishers Inc, New York.
- Ruiz-Hitzky, E., Darder, M., Wicklein, B., Castro-Smirnov, F.A., Aranda, P., 2019. Clay-based biohybrid materials for biomedical and pharmaceutical applications. Clays Clay Miner. 67, 44–58. https://doi.org/10.1007/s42860-019-0005-0.
- Sawangchan, P., Alexandrino Júnior, F., Alencar, É.N., Egito, E.S.T., Kirsch, L.E., 2023. The role of aggregation and ionization in the chemical instability of Amphotericin B in aqueous methanol. Int. J. Pharm. 632, 122586. https://doi.org/10.1016/j.ijpharm.2023.122586.
- Scolding, P., Fahal, A., Yotsu, R.R., 2018. Drug therapy for Mycetoma. Cochrane Database of Systematic Reviews CD013082.
- Shukla, P.K., Singh, P., Yadav, R.K., Pandey, S., Bhunia, S.S., 2016. Past, present, and future of antifungal drug development. In: Topics in Medicinal Chemistry. pp. 125–167. Doi: 10.1007/7355_2016_4.

- Sow, D., Ndiaye, M., Sarr, L., Kanté, M.D., Ly, F., Dioussé, P., Faye, B.T., Gaye, A.M., Sokhna, C., Ranque, S., Faye, B., 2020. Mycetoma epidemiology, diagnosis management, and outcome in three hospital centres in Senegal from 2008 to 2018. PLoS One 15, e0231871. https://doi.org/10.1371/journal.pone.0231871.
- Trikeriotis, M., Ghanotakis, D.F., 2007. Intercalation of hydrophilic and hydrophobic antibiotics in layered double hydroxides. Int. J. Pharm. 332, 176–184. https://doi. org/10.1016/j.ijpharm.2006.09.031.
- van de Sande, W.W.J., 2013. Global burden of human mycetoma: a systematic review and meta-analysis. PLoS Negl. Trop. Dis. 7, e2550.
- Wang, X., Mohammad, I.S., Fan, L., Zhao, Z., Nurunnabi, M., Sallam, M.A., Wu, J., Chen, Z., Yin, L., He, W., 2021. Delivery strategies of amphotericin B for invasive fungal infections. Acta Pharm. Sin. B 11, 2585–2604. https://doi.org/10.1016/j. apsb.2021.04.010.
- Wasko, P., Luchowski, R., Tutaj, K., Grudzinski, W., Adamkiewicz, P., Gruszecki, W.I., 2012. Toward understanding of toxic side effects of a polyene antibiotic amphotericin B: fluorescence spectroscopy reveals widespread formation of the specific supramolecular structures of the drug. Mol. Pharm. 9, 1511–1520. https:// doi.org/10.1021/mp300143n.

- Welsh, O., Al-Abdely, H.M., Salinas-Carmona, M.C., Fahal, A.H., 2014. Mycetoma medical therapy. PLoS Negl. Trop. Dis. 8, e3218.
- World Health Organization (WHO) (Ed.), 2022. WHO fungal priority pathogens list to guide research, development and public health action. Geneva.
- World Health Organization (WHO) (Ed.), 2016. Addressing the burden of mycetoma. In: Sixty-Ninth World Health Assembly. Geneva. pp. 50–52.
- Yang, J.-H., Lee, J.-H., Ryu, H.-J., Elzatahry, A.A., Alothman, Z.A., Choy, J.-H., 2016. Drug-clay nanohybrids as sustained delivery systems. Appl. Clay Sci. 130, 20–32. https://doi.org/10.1016/j.clay.2016.01.021.
- Yu, Y., Chen, P., Gao, M., Lan, W., Sun, S., Ma, Z., Sultani, R., Cui, Y., Umar, M.N., Khan, S.W., Cai, X., Liang, Z., Tan, H., 2022. Amphotericin B tamed by salicylic acid. ACS Omega 7, 14690–14696. https://doi.org/10.1021/acsomega.1c07201.
- Zein, H.A.M., Fahal, A.H., Mahgoub, E.S., Hassan, T.A.E., Abdel-Rahman, M.E., 2012. Predictors of cure, amputation and follow-up dropout among patients with mycetoma seen at the Mycetoma Research Centre, University of Khartoum, Sudan. Trans. R. Soc. Trop. Med. Hyg. 106, 639–644. https://doi.org/10.1016/j.trstmh.2012.07.003.